Volume 17
Number 30
14 August 2025
Pages 6145–6256

# Analytical Methods

rsc.li/methods

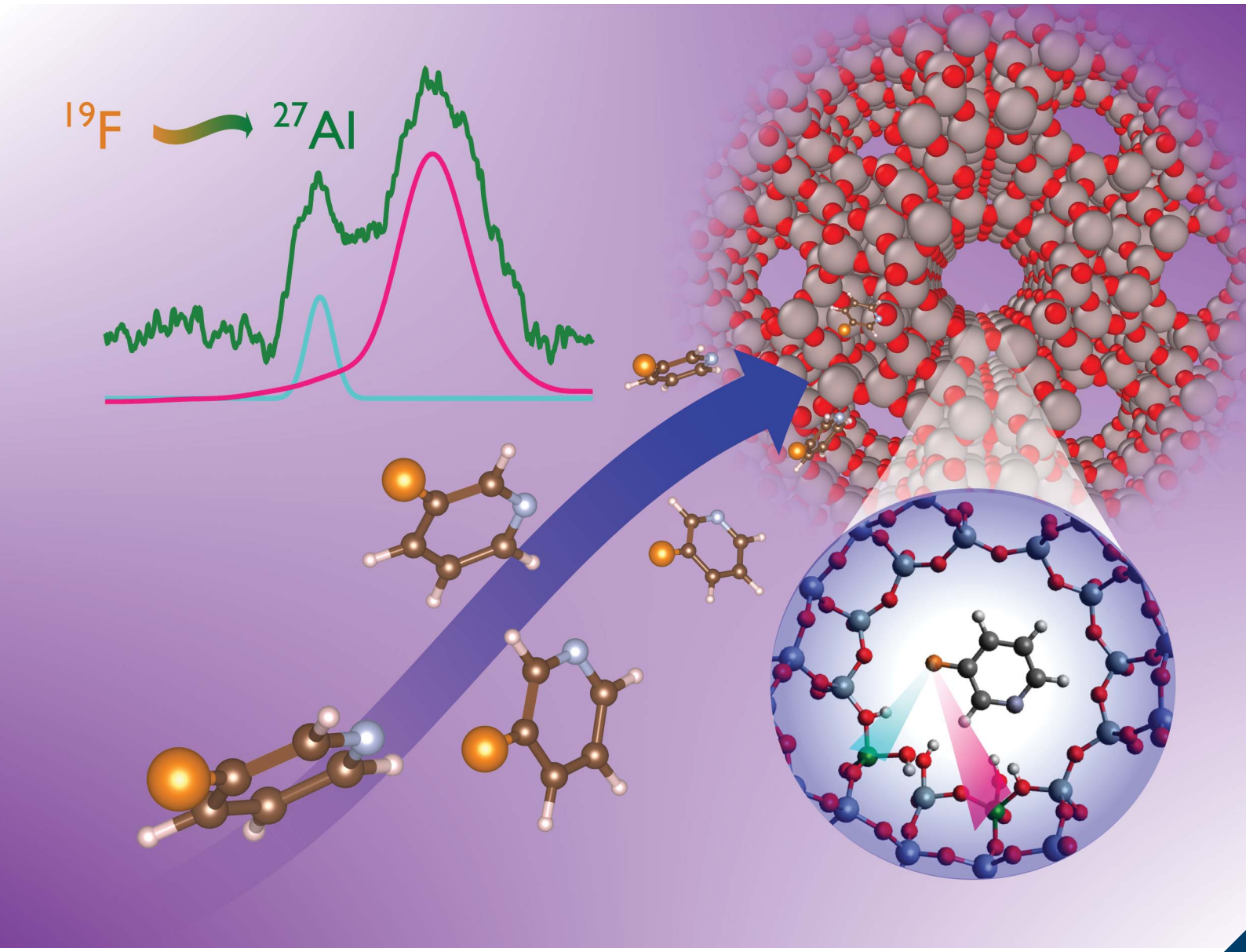


ISSN 1759-9679

ROYAL SOCIETY OF CHEMISTRY

**PAPER**
Daniel Lee *et al.*
Exposing active sites in zeolites with fluoropyridines as NMR probe molecules

Indexed in Medline!

Analytical Methods

PAPER

View Article Online
View Journal | View Issue



Cite this: *Anal. Methods*, 2025, **17**, 6151

# Exposing active sites in zeolites with fluoropyridines as NMR probe molecules†

Joseph Hurd,[a] Yujie Ma,[b] Paolo Cerreia Vioglio,[c] Run Zou,[a] Dinu Iuga,[d] Sihai Yang,[be] Xiaolei Fan[af] and Daniel Lee*[a]

Received 26th March 2025
Accepted 30th June 2025

DOI: 10.1039/d5ay00507h

rsc.li/methods

Active sites in zeolites are crucial for catalysis, but their identification remains challenging due to structural complexity. Solid-state NMR, a key tool for studying zeolites, can struggle with directly detecting acidic properties due to the quadrupolar nature of ubiquitous metal dopants. Here, we use fluorinated pyridine as a probe to identify active sites in HY and HZSM-5, two important solid acid catalysts. $^{19}$F NMR effectively detects binding environments, while $^{19}$F–$^{27}$Al polarization transfer reveals elusive penta-coordinated Al$^{V}$ Brønsted acid sites and shows that the dominant active sites are distorted framework-associated Al$^{IV}$ and Al$^{V}$ sites with large quadrupolar coupling constants, shedding light on catalytic properties. Low-temperature (100 K) NMR proves essential for capturing these interactions. This work enhances the understanding of zeolite active sites and highlights the broad applicability of fluorinated probe molecules for surface characterization, offering a cost-effective, highly sensitive approach for catalytic studies.



## Introduction

Zeolites are the most widely used catalyst class for the cracking of hydrocarbons.[1–4] They also show promise for methanol-to-olefin (MTO) fuel production and for the processing of other types of renewable biomass into usable fuels and products,[5–8] as well as for the upcycling of polyolefin plastics.[9–11] Starting from a porous silica ($SiO_2$) structure, doping of metals such as Al into the zeolite framework introduces acid sites that can be active for catalysis.[6,12–15] Much work over many decades has been undertaken to try to optimise the framework structures and pore sizes,[16–20] the amount of acid sites, the ratio of types of acid sites (Brønsted : Lewis),[21,22] and also the synergy between different acid sites and dopants (such as single atoms sites[23–25] or nanoparticles[26,27]) for particular applications. Therefore, knowledge of how the atomic-level structure relates to catalytic mechanisms is essential.

Solid-state NMR (ssNMR) spectroscopy can provide local information about $^{1}$H,[28–30] $^{29}$Si,[31–33] $^{17}$O,[34–36] and $^{27}$Al[28–32,37] sites. Although Al (and other metals) can be inserted into the framework in tetrahedral (Al$^{IV}$) positions, it is well known that there are a number of different extra-framework aluminium (EFAl) sites present in such materials: Al$^{IV}$, penta-coordinated Al$^{V}$, and hexa-coordinated Al$^{VI}$.[14,32,38] Different synthesis/doping methods and post synthetic treatments have been applied to change the silicon : aluminium ratio (SAR) of zeolites as well as their pore structures, thus varying the Brønsted acid site (BAS) : Lewis acid site (LAS) ratio and their accessibilities.[30] This leads to different functional properties.

Computational chemistry techniques have been applied to model how reagents bind, elucidating reaction pathways,[39–41] and to investigate the types of active site present,[42–45] so that structure can be related to function. Nevertheless, the nature of some of these sites remains ambiguous even after frequent investigations. One such site is the penta-coordinated EFAl$^{V}$ moiety;[32,46] it has generally been treated as a LAS and its distorted geometry leads to it being a highly active species.[47–49] However, recent work from Deng and coworkers suggests that there is also the potential for BAS-type activity for Al$^{V}$ sites.[32] Structural ambiguities such as these hinder a comprehensive understanding of the catalytic activity of these vital porous materials.

Analysis using adsorption of probe molecules can give the types and relative strengths of the acid sites present. Probe molecules are commonly used with IR spectroscopy, temperature programmed desorption (TPD), as well as NMR spectroscopy. For NMR, the main probe molecules can be split into two

[a]*Department of Chemical Engineering, The University of Manchester, Oxford Road, Manchester M13 9PL, UK. E-mail: daniel.lee@manchester.ac.uk*
[b]*Department of Chemistry, The University of Manchester, Oxford Road, Manchester M13 9PL, UK*
[c]*Sir Peter Mansfield Imaging Centre, The University of Nottingham, Nottingham NG7 2RD, UK*
[d]*Department of Physics, The University of Warwick, Coventry CV4 7AL, UK*
[e]*College of Chemistry and Molecular Engineering, BNLMS, Peking University, 202 Chengfu Road, Haidian, Beijing 100871, China*
[f]*Ningbo China Beacons of Excellence Research and Innovation Institute, University of Nottingham Ningbo China, 211 Xingguang Road, Ningbo 315048, China*

† Electronic supplementary information (ESI) available. See DOI: https://doi.org/10.1039/d5ay00507h

categories derived from their NMR-active isotopes used to characterise surfaces: $^{31}$P-based, *e.g.* trimethylphosphine (TMP) and trimethylphosphine oxide (TMPO),[50,51] and $^{15}$N-based, *e.g.* pyridine (Py).[50] These are used because they interact strongly with active sites and their spy nuclei have high sensitivities to environmental changes owing to large chemical shift ranges. However, TMP and TMPO are hazardous (TMP is highly toxic and flammable).[21,51,52] Py is commonly used with FT-IR to give rapid assignment of acid sites and their strengths. Ammonia and Py have proven to be particularly useful for the characterization of acid sites through the combination of FT-IR and TPD for quasi-quantitative assignment of site coverage.[53–59] Ammonia can be preferred for TPD owing to its lower cost, smaller size, lower desorption temperatures, and reduced hazards compared to Py. The utility of Py as a probe molecule with NMR spectroscopy has been recently highlighted for example by Copéret and coworkers who used adsorption of $^{15}$N-enriched Py combined with variable temperature $^{15}$N NMR and DFT studies to elucidate the presence of a pseudo tricoordinated framework-associated LAS in the zeolite mordenite.[46] Its distorted nature suggests that it is likely very active in catalysis, but this needs to be further investigated.[46] The use of isotopically-enriched Py was required as $^{15}$N has low NMR receptivity (0.04% compared to $^{1}$H) but $^{15}$N-Py is costly (~2 k€ per g).

Both categories of probe molecule exhibit multiple binding modes. TMPO adsorbs to both BAS and LAS and shows a total of 4 LAS and BAS coordination modes/strengths for zeolite Y (H form, HY)[52,60] and binding to 5 different BASs for HZSM-5.[51] The relative spatial proximities between the active sites can be determined using 2D correlation NMR spectroscopy involving $^{31}$P from TMPO.[60] Similarly, monomethylamine (MMA) studies for HZSM-5 and HY have been used to examine spatial correlations whilst showing multiple binding sites for both zeolites.[53,61] Combining NMR spectroscopy of probe molecules with synchrotron resonant soft X-ray diffraction and neutron powder diffraction has very recently enabled the identification of the specific locations of tetrahedral framework aluminium in HZSM-5 [62] but not framework-associated or extra-framework sites owing to their lack of long-range order.

Similar to $^{31}$P, $^{19}$F has favourable NMR properties, including high receptivity (>12 times that of $^{31}$P) and a wide chemical shift range. Fluorine is also predominantly found naturally only in minerals, so it rarely contributes to signals from most synthetic zeolitic analytes and thus resonance overlap is minimal, and resolution is high. This means that it is in principle an ideal spy nucleus; indeed, 4-fluoronitrobenzene and 4-fluoroaniline have been used to measure zeolite acidity,[63] 4-fluoroacetophenone has been used to do so quantitatively,[64,65] and $CF_4$ has been used to probe pore dimensions and accessibility in a similar manner to $^{129}$Xe NMR,[66] while ammonium hexafluorosilicate has been used to investigate dealumination processes.[67] Functionalised pyridines containing $^{19}$F such as 2- and 3-fluoropyridine (2FP and 3FP, respectively) are widely commercially available at low cost (~10 € per g). TPD experiments have shown that they bind to active sites in zeolites[68] and therefore they have the potential to be useful probe molecules for NMR.

Herein, the utility of fluoropyridines as NMR probe molecules is demonstrated. Zeolites HY (SAR = 2.6) and HZSM-5 (SAR = 40) were selected as the focus of this investigation due to their wide industrial relevance[69–73] as well as both having similar active sites but different pore sizes, structures, and active site distributions. Pyridine has a kinetic diameter of ~5.3 Å, so it can fit into the medium-sized pores of the 10-membered rings (10-MR) (~5.5 Å) of HZSM-5 (ref. 74) but will be tightly constrained by the small size (see Fig. 1). Pyridine fits more easily into the large-pore 12-MR supercages of HY (pore opening ~7.4 Å). However, pyridine is too large to fit into the smaller sodalite cages of HY. Here, high-field NMR and low temperature NMR are used for increased resolution and sensitivity, respectively, enabling multiple binding modes/strengths to be detected for fluoropyridines adsorbed on HY and HZSM-5 *via* $^{19}$F NMR. Notably, polarisation transfer from the probe molecule ($^{19}$F) to the zeolites ($^{27}$Al) has shown the unexpected presence of pentacoordinated framework-associated BAS and that these are the preferred adsorption sites for both zeolites. This highlights the importance of using probe molecules to gain detailed insights into the active sites so that structure can be related to function and thus so that structures can be effectively rationally optimised.

## Results and discussion

Pyridine is commonly used as a probe molecule for IR studies of active sites in zeolites since the resulting spectra can be used to discriminate between protonated pyridine (Py-H$^+$), pyridine adsorbed at a weak BAS through H-bonding (Py-B), and pyridine adsorbed at a LAS (Py-L).[75,76] Fig. 1 shows the absorbance-mode FT-IR spectral region of 1800–1350 cm$^{-1}$ for HY and HZSM-5 dosed with 2FP and 3FP as well as the pure zeolites and fluoropyridines, for comparison. The peaks observed for the 2FP-dosed zeolites are very similar to those expected for equivalent Py adsorption. These show clear protonated species (2FP-H$^+$@HY and 2FP-H$^+$@HZSM-5) and adsorption at LAS (2FP-L@HY and 2FP-L@HZSM-5) for both zeolites. 3FP does not have the same spectral separation of ($\nu_{8a}$) vibrational modes as Py or 2FP but the 3FP-dosed zeolites exhibit bands corresponding to 3FP-H$^+$ with higher wavenumbers (1565 cm$^{-1}$ for HY and 1571 cm$^{-1}$ for HZSM-5; *cf.* 1547 and 1543 cm$^{-1}$ for 2FP-dosed zeolites, respectively) and bands corresponding to adsorption at weak LAS with lower wavenumbers (1434 cm$^{-1}$ for HY and 1433 cm$^{-1}$ for HZSM-5; *cf.* 1440 and 1439 cm$^{-1}$ for 2FP-dosed zeolites, respectively). This suggests that 2FP and 3FP have different adsorption geometries and/or binding strengths and these are dependent on the type of active site. These variations highlight the sensitivity of fluoropyridines as probe molecules.

As the FT-IR spectra demonstrated that both 3FP and 2FP bind to active sites in zeolites HY and HZSM-5, they were both investigated using conventional $^{19}$F solid-state NMR spectroscopy at 9.4 T field strength. A TPD study shows different preferential bindings for 2FP and 3FP to zeolite acid sites in HZSM-5 and H-Mordenite with 3FP having a higher adsorption enthalpy.[68] Disappointingly, the {$^{1}$H–}$^{19}$F cross-polarisation

 

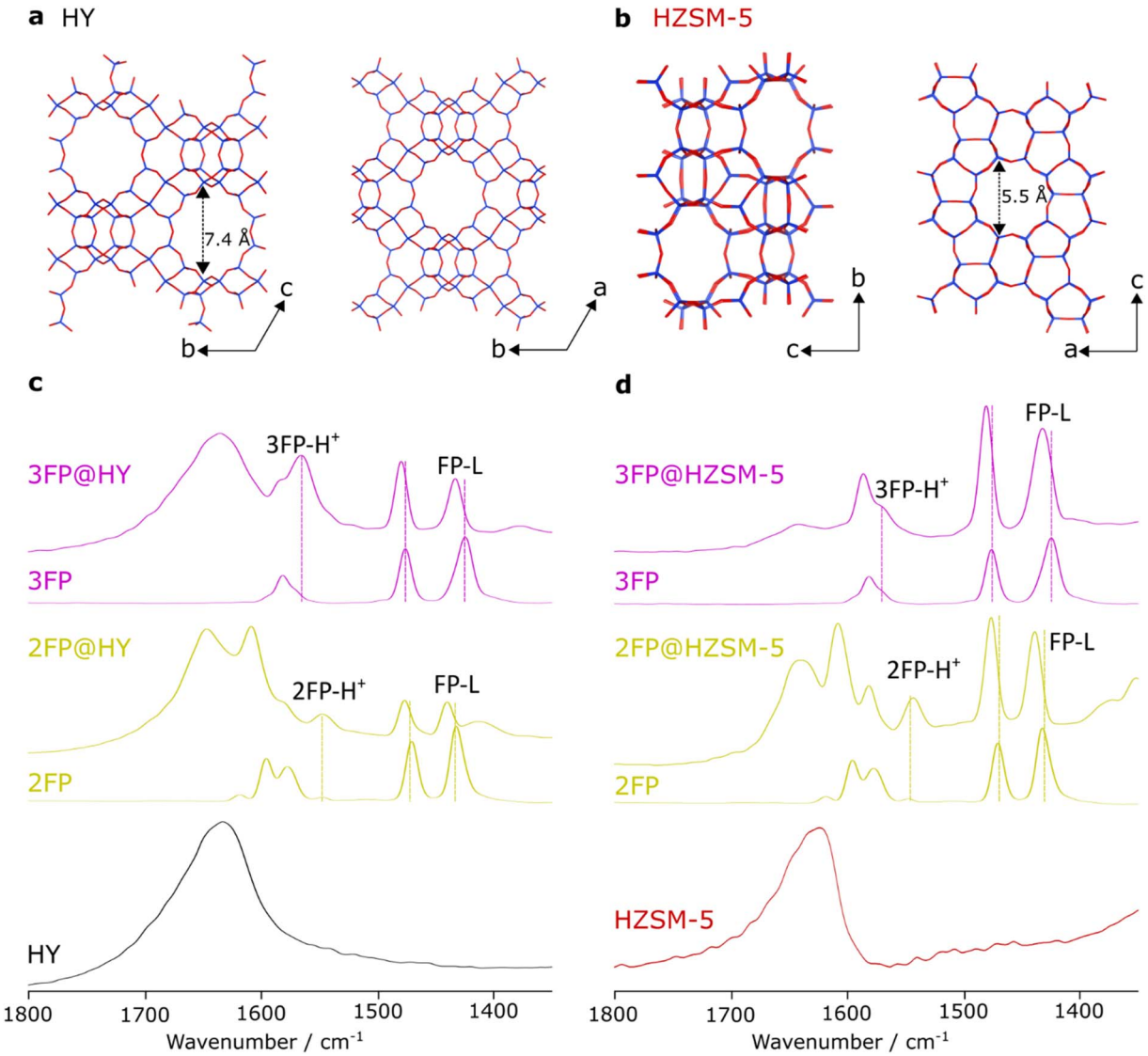


Fig. 1 Structures of zeolite Y (a) and ZSM-5 (b); only oxygen (red) and silicon/aluminium (blue) sites are represented. FT-IR spectra (c and d) of zeolite HY (c) and zeolite HZSM-5 (d), dosed with 3FP (top), 2FP (middle) and undosed (bottom) with relevant acid site bindings shown on the spectra. Wavenumbers and assignment are tabulated in Table S7.†

magic angle spinning (CPMAS) NMR spectra of 2FP@HY and 2FP@HZSM-5 are almost identical (see Fig. S1†). They both show a large component ($\delta\{^{19}F\} \approx -70$ ppm) and two smaller components ($\delta\{^{19}F\} \approx -70$ and $-80$ ppm), with the smaller components exhibiting sizeable chemical shift anisotropies (CSA). Cross-polarisation was used to be selective to species that are strongly adsorbed; CPMAS uses the dipolar interaction (here between $^{1}H$ and $^{19}F$) to transfer polarisation between spins and this can be averaged-out under fast isotropic motion, leading to poor transfer efficiencies. Nevertheless, the larger peak displays negligible CSA, indicating dynamical averaging (see Fig. S1 and Table S8†). Thus, this larger peak can be assigned to physisorbed species and the smaller peaks to species bound to active sites. Although CPMAS is not inherently quantitative, $^{19}F$ direct excitation with careful sample preparation can enable a quantitative analysis of acid sites, as has been shown previously.[64]

The $\{^{1}H–\}^{19}F$ CPMAS NMR spectra of 3FP@HY and 3FP@HZSM-5 are substantially different, even at moderate field strengths (9.4 T, see Fig. 2, S1, and S2†). This is a first indication that 3FP can be used to differentiate active sites between similar zeolite solid acid catalysts. For 3FP, however, the smaller, broader, higher anisotropy peaks are deshielded (*i.e.* higher ppm) compared to the narrower peaks from physisorbed species ($\delta\{^{19}F\} \approx -130$ ppm). This infers, as expected, that the position of the F on the pyridine ring (*e.g.* 2FP *vs.* 3FP) plays a role in the electronic interaction of the probe molecule with the zeolite surface and this is reflected in its chemical shielding. The direct excitation $^{19}F$ MAS NMR spectra of 3FP@HY and 3FP@HZSM-5 (Fig. 2) are similar to the respective CPMAS NMR spectra but it is clear from the reduced relative presence of spinning side bands that there is a large proportion of dynamic species that are not detected *via* CP. However, comparing these

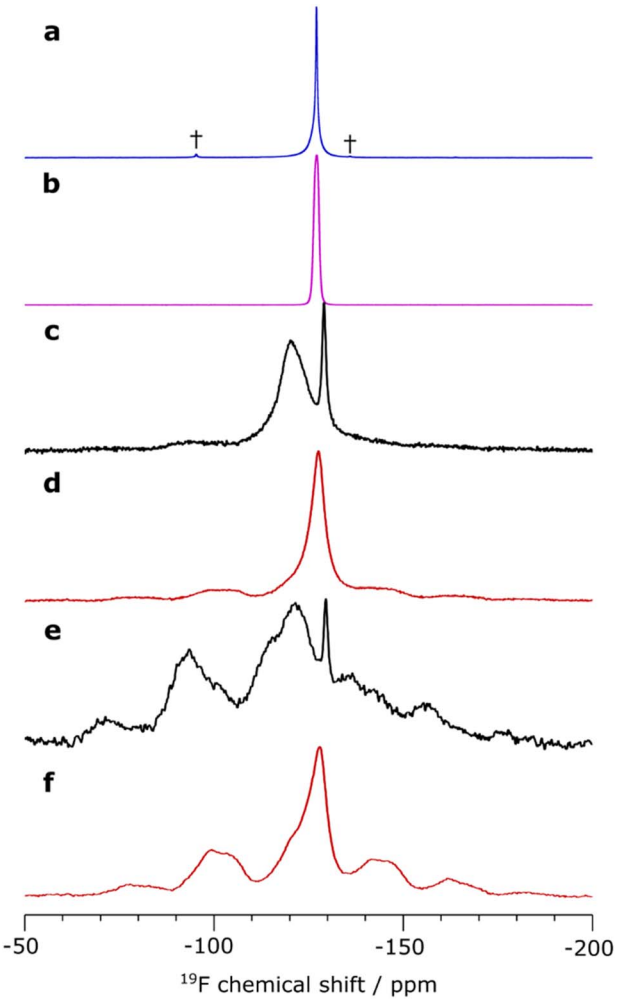


Fig. 2 9.4 T $^{19}$F direct excitation (a–d) and {$^{1}$H–}$^{19}$F CP (e and f) MAS NMR spectra recorded with $^{1}$H decoupling at ambient temperature. Spectra shown are of 3FP-doped samples of silicalite-1 (blue) (a), γ-alumina (purple) (b), HY (black) (c and e), and HZSM-5 (red) (d and f). † Denotes artifacts from decoupling. (a and b) were recorded with 12 kHz MAS frequency and (c–f) were recorded with 8 kHz MAS frequency.

spectra to those of 3FP@silicalite-1 (a pure silica MFI-type zeolite) and 3FP@γ-alumina (a nanoparticulate Lewis acid catalyst) shows that 3FP interacts strongly with acid sites in the porous acid catalysts since the $^{19}$F resonances for 3FP@silicalite-1 and 3FP@γ-alumina correspond to mainly physisorbed species (Fig. 2a and b). Since 3FP shows a greater difference for $^{19}$F NMR spectra between HY and HZSM-5 compared to 2FP, 3FP will be the focus of the rest of the study.

To reduce the dynamics of adsorbed 3FP, the doped zeolites were cooled to 260 K. Very similar {$^{1}$H–}$^{19}$F CPMAS NMR spectra are observed compared to those recorded at ambient temperatures (Fig. S2†). However, there are some notable differences. The $^{19}$F resonances assigned to physisorbed 3FP have become broader and now present a larger CSA, as would be expected with reduced dynamics. The highest shifted (most down-field) $^{19}$F isotropic resonance observed for 3FP@HZSM-5 appears at a lower chemical shift compared to 3FP@HY (*cf.* $\delta\{^{19}F\} \approx -118$ ppm for HZSM-5 and −112 ppm for HY) but it has very similar CSA parameters: $\delta_{CSA}$ and $\eta$ (see Fig. 2, S1, and S2, and Table S8†). This indicates that 3FP is adsorbed in a similar mode, but with a different strength. Notably, there are $^{19}$F resonances observed with intermediate chemical shifts ($\delta\{^{19}F\} \approx -120$ to −128 ppm), and the associated CSA tensors have asymmetry parameters, $\eta$, close to 1, whereas the highest shifted resonances have asymmetry parameters closer to 0; this indicates that the binding mode that results in the corresponding $^{19}$F CSA tensor is very different. Previous $NH_3$-TPD measurements on HY (with the silicon-to-aluminium ratio, SAR, = 2.6) show a balanced weak : strong acidity (0.8 : 1.0) where the total active acidity is from a 1.0 : 1.1 BAS : LAS ratio and that the majority of LAS show weak acidity whereas the BAS show strong acidity.[77] For HZSM-5 with lower Al content (SAR = 38), $NH_3$-TPD studies show a greater proportion of BAS compared to LAS and weaker LAS but stronger BAS than HY.[78] Therefore, it is likely that the downfield $^{19}$F resonances stem from 3FP-L and the intermediate $^{19}$F resonances stem from 3FP-B owing to their relative amounts in each zeolite (Table S8†) and that downfield shifts (higher ppm) indicate greater acid strengths. The $^{19}$F spectrum and resonances are generally broader for 3FP@HY compared to 3FP@HZSM-5. This is consistent with the $NH_3$-TPD analysis that highlights the complexity and variation of acidic strength of HY,[78,79] leading to a distribution of $^{19}$F chemical shifts that are not dynamically averaged. Therefore, NMR chemical shifts and their anisotropies from 3FP $^{19}$F resonances can be used to distinguish LAS and BAS in zeolites, as well as their strengths, with higher deshielding (more positive ppm) stemming from both stronger binding and from 3FP-L.

The impact of the 3FP doping can also be observed *via* $^{27}$Al MAS NMR spectra (Fig. S3†). Framework tetrahedral aluminium-27 resonances ($\delta\{^{27}Al\} \approx 60$ ppm) are perturbed upon adsorption of 3FP. For both zeolites there is a slight broadening of these signals, particularly at the high-field (lower ppm) side, and this effect is larger for HY than HZSM-5. Furthermore, the resonances corresponding to hexa-coordinated extra-framework aluminium ($EFAl^{VI}$) species ($\delta\{^{27}Al\} \approx 0$ ppm) for both zeolites, which are much more prevalent in HY, are reduced upon adsorption of 3FP. This is likely due to direct binding of 3FP to these LAS (*vide supra*) or 3FP may lead to an annealing effect on the zeolites as pyridines can help relax distorted Al centres.[46]

To gain higher spectral resolution from 3FP adsorbed on the zeolites, high-field (20.0 T) NMR analysis was employed and combined with fast MAS (33 kHz). It is clear from high-resolution $^{1}$H MAS NMR spectra recorded at ∼260 K (Fig. S4†) that a highly acidic proton is observed ($\delta\{^{1}H\} \approx 15$ ppm) upon adsorption of 3FP to zeolite HY. A similar chemical shift is observed ($\delta\{^{1}H\} \approx 15$ ppm) for $d_5$-pyridine adsorbed to HY and is assigned to Py-$H^+$.[32] The assignment to 3FP-$H^+$ is confirmed here through a $^{1}$H–$^{1}$H dipolar correlation spectrum (Fig. S5†), which shows a correlation for this resonance with 3FP protons. The absence of a similar peak for 3FP@HZSM-5 is attributed to the lower amount of BAS compared to HY. It is also clear that

 

the $^{1}$H from 3FP are more dynamic for 3FP@HZSM-5 compared to 3FP@HY, as demonstrated by the narrower associated resonances ($\delta\{^{1}H\} \approx 6$–$10$ ppm). This is consistent with the analysis of the 9.4 T 260 K $\{^{1}H–\}^{19}F$ CPMAS NMR spectra (*vide supra*). This could be considered counterintuitive since the pores of HZSM-5 are smaller than those of HY and thus 3FP should be more tightly constrained in the former. This infers that 3FP interacts more strongly with the pores in HY, either due to the nature of the active sites or to the larger proportion of these. Ambient temperature high-field acquisition of $\{^{1}H–\}^{19}F$ CPMAS NMR spectra of 3FP@HY and 3FP@HZSM-5 was challenging. This again highlights the mobility of 3FP in the pores. With cooling (~260 K), to counteract frictional sample heating under MAS, high-resolution $\{^{1}H–\}^{19}F$ CPMAS NMR spectra could be obtained (Fig. 3). Deconvolution of the 3FP@HY $^{19}$F NMR spectrum shows two clusters of peaks ($\delta\{^{19}F\} \approx -104$ to $-116$ ppm and $-118$ to $-134$ ppm). Even at high-field with fast MAS, the $^{19}$F resolution is not sufficient to resolve individual peaks; the deconvolution is non-definitive but has been fit with the minimum number of peaks required for a suitable reproduction of the spectrum (full fitting parameters can be found in Table S10†). This deconvolution demonstrates the benefits of high-field as it is evident that there are multiple $^{19}$F resonances and thus adsorption modes/strengths. As noted above, the downfield (higher ppm) cluster is assigned to 3FP-L and the upfield cluster is from 3FP-B and physisorbed 3FP. For 3FP@HZSM-5 the observed $^{19}$F chemical shift range is more limited but there are still two discrete clusters ($\delta\{^{19}F\} \approx -114$ to $-120$ ppm and $-120$ to $-134$ ppm), with the downfield and upfield clusters assigned to 3FP-L and 3FP-B/physisorbed, respectively (*vide supra*). The sample cooling has provided further evidence for 3FP adsorption to strong BAS through the formation of 3FP-H$^{+}$ and, combined with high-fields, the $^{19}$F NMR spectra show that there are a variety of binding modes and strengths at both LAS and BAS and that the variety is greater for HY compared to HZSM-5, as is the strength of LAS.

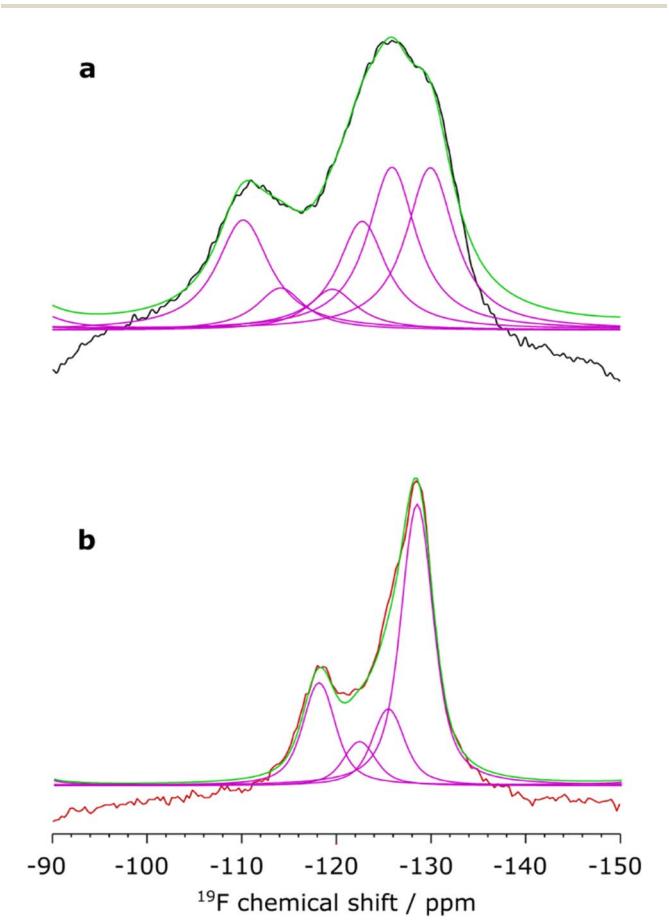


Fig. 3 20 T $\{^{1}H–\}^{19}F$ CPMAS NMR spectra recorded with cooling (~260 K) and using a MAS frequency of ~33 kHz. Spectra shown are of (a) 3FP-dosed zeolite HY (black) and (b) 3FP-dosed HZSM-5 (red), with deconvolutions (purple) and the envelope (green). Fitted parameters are given in Table S10.†

Pyridine has previously been shown to adsorb to common zeolites with multiple binding modes.[58,76] This is consistent with the number of major adsorption sites found for 3FP for the two zeolites studied herein. To further reduce the dynamics of adsorbed 3FP and also to increase the NMR sensitivity, MAS NMR spectra were collected at 100 K and 14.1 T. This enabled $\{^{19}F–\}^{27}Al$ CPMAS NMR spectra to be recorded (Fig. 4), which show where 3FP is adsorbed in the zeolites; this was not possible previously at higher temperatures owing to reduced experimental sensitivity (Fig. S6†). As expected, $^{27}$Al resonances are detected near $^{19}$F spins at $\delta\{^{27}Al\} \approx 60$ ppm for both HY and HZSM-5, which correspond to 3FP-B since these BAS arise from framework tetrahedral Al$^{IV}$. These $^{27}$Al resonances can be deconvoluted into two contributions: (i) framework Al$^{IV}$-1 ($C_Q \approx 2.9$ MHz, $\delta_{iso}\{^{27}Al\} \approx 64$ ppm) and (ii) framework-associated Al$^{IV}$-2 ($C_Q \approx 6.4$ MHz, $\delta_{iso}\{^{27}Al\} \approx 65$ ppm).[38,47,80] Their relative contributions to the $\{^{19}F–\}^{27}Al$ CPMAS NMR spectra (1.0 : 1.2 for HY and 1 : 2 for HZSM-5, see Table S11†) are different compared to the quantitative direct excitation $^{27}$Al MAS NMR spectra (1.0 : 0.5 for undosed HY and 1.0 : 0.4 for undosed HZSM-5, Fig. S9 and Table S12†). This demonstrates that 3FP adsorbs near Al$^{IV}$-2 sites more preferentially than near Al$^{IV}$-1 sites. This could be expected since these sites protrude into the pores and have been shown to be responsible for enhanced catalytic activity.[80] It is notable that the relative intensity of 3FP adsorption to Al$^{IV}$-2 compared to Al$^{IV}$-1 is greater for HZSM-5 compared to HY; this may explain the results of calorimetry studies of the two zeolites which show greater pyridine adsorption enthalpy for HZSM-5 than HY.[81]

Surprisingly, and importantly, a different $^{27}$Al resonance is detected ($\delta\{^{27}Al\} \approx 20$ ppm) as the primary adsorption site for 3FP in both zeolites (~8 : 1 compared to Al$^{IV}$-1). This resonance is not detected in direct excitation $^{27}$Al MAS NMR spectra nor in a $^{1}$H–$^{27}$Al dipolar correlation MAS NMR spectrum, even at high field (see Fig. S10 and S11†); only an Al$^{V}$ site stemming from EFAl$^{V}$ is detected for HY ($\delta\{^{27}Al\} \approx 30$ ppm). This demonstrates the utility of $\{^{19}F–\}^{27}Al$ CP with adsorbed 3FP to reveal previously undetectable Al sites; they are likely scarce yet have a high propensity for adsorption. To assign this resonance to 3FP-B or 3FP-L, a complementary $^{15}$N NMR spectrum was recorded for 3FP@HY (Fig. 4c). Owing to the low NMR receptivity of $^{15}$N (*e.g.* natural isotopic abundance of 0.4%), the $\{^{1}H–\}^{15}N$ CPMAS NMR spectrum was enhanced using dynamic nuclear

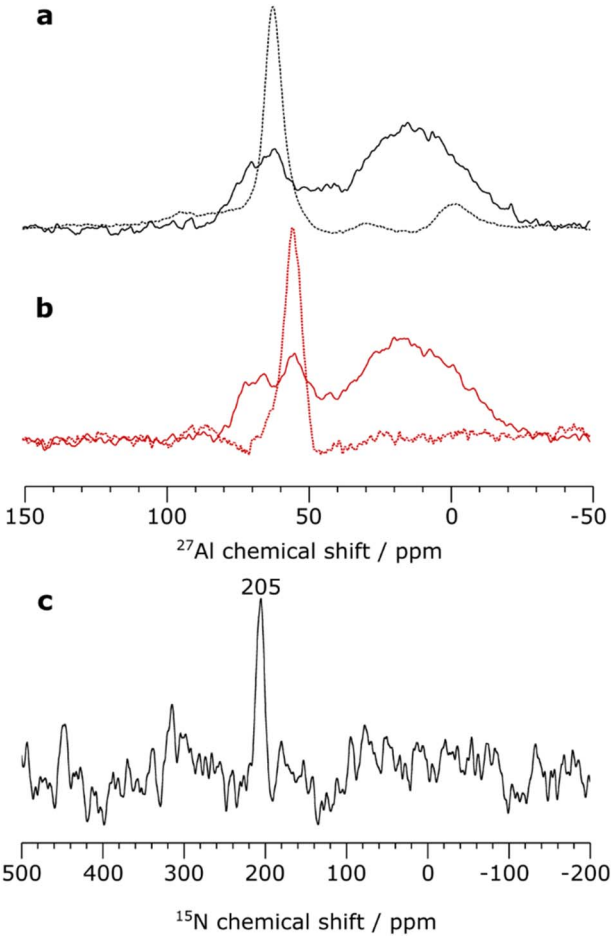


Fig. 4 14.1 T, 100 K $\{^{19}F–\}^{27}Al$ CPMAS NMR spectra (a and b) and DNP-enhanced $\{^{1}H–\}^{15}N$ CPMAS NMR spectrum (c) of 3FP-dosed zeolites HY (black) (a and c) and HZSM-5 (red) (b). The corresponding $^{27}Al$ direct excitation MAS NMR spectra are shown with dashed lines in (a and b) and spectral deconvolutions are given in Fig. S8.† The MAS frequency was 8 kHz for all spectra and $^{27}Al$ background correction is shown in Fig. S7.†

polarization.[82–84] The resulting spectrum shows a single $^{15}N$ resonance ($\delta\{^{15}N\} \approx 205$ ppm) that corresponds to Py-B.[58,59] There is no observed signal for Py-L (expected $\delta\{^{15}N\} \approx 240$ ppm[46,85]). Therefore, the primary adsorption site for 3FP is a BAS with low $^{27}Al$ chemical shift.

Recent studies have presented active sites in zeolites that could be responsible for the primary adsorption site for 3FP. Yakimov *et al.* used adsorption of pyridine on mordenite zeolite combined with low temperature MAS NMR spectroscopy and DFT calculations and showed that Py-B ($C_Q \approx 1.8$ MHz, $\delta_{iso}\{^{27}Al\} \approx 54$ ppm) were prevalent and that framework-associated pseudo tri-coordinated Al LAS existed and could also adsorb Py ($C_Q \approx 9.4$ MHz, $\delta_{iso}\{^{27}Al\} \approx 58$ ppm).[46] Zheng *et al.* also used Py-adsorption but for HY and with 2D correlation MAS NMR spectroscopy demonstrated the existence of unprecedented penta-coordinated $Al^V$-BAS ($C_Q \approx 5.6$ MHz, $\delta_{iso}\{^{27}Al\} \approx 35$ ppm).[32] The latter study was performed at room temperature, and it is known that quadrupolar parameters can be dynamically averaged.[46] The values extracted from our low temperature measurements (Table S11†) for the primary adsorption site for 3FP on HY and HZSM-5 ($C_Q \approx 7.5$ MHz, $\delta_{iso}\{^{27}Al\} \approx 30$ ppm) match well to those reported for $Al^V$-BAS, accounting for reduced dynamics. Moreover, a very recent theoretical and experimental study by Wang *et al.*[86] showed that "NMR-invisible" tri-coordinated Al sites in ultrastable Y (USY) zeolite become detectable upon hydration and that this adsorption of water leads to framework-associated $Al^{IV}$-2 and, importantly, $Al^V$-BAS ($C_Q \approx 9.3$ MHz, $\delta_{iso}\{^{27}Al\} \approx 32$ ppm). USY is prepared from HY *via* calcination that dealuminates the framework, creating tri-coordinated Al defects. Therefore, the evidence here suggests that these sites can also be found in HY and HZSM-5 in low concentrations and that adsorption of 3FP is preferentially to these difficult-to-detect $Al^V$-BAS structures and $\{^{19}F–\}^{27}Al$ CPMAS NMR facilitates this observation. This highlights the challenge of correlating structure with activity in heterogeneous catalysts. However, probe molecules can effectively target active sites and, when combined with solid-state NMR analysis, provide detailed insights into the accessibility and acidity of these sites.

## Conclusion

This study demonstrates the efficacy of 3-fluoropyridine (3FP) as a powerful probe molecule for elucidating the nature of active sites in zeolites (exemplified by HY and HZSM-5). 2-fluoropyridine (2FP) was also investigated but shows inferior properties compared to 3FP in terms of adsorption strength and resulting $^{19}F$ chemical shift perturbations. Nevertheless, it may find value for certain applications. The advantages of 3FP are that: (i) it is readily applicable as a probe molecule for a variety of analytical tools including TPD, IR, and NMR, facilitating complementary characterisations; (ii) it is relatively inexpensive; (iii) it is relatively small so can fit in micropores; (iv) it can bind (as Py does) to both BAS and LAS; and (v) it can differentiate acid strengths through chemical shifts of both $^{15}N$ and $^{19}F$. The limitations are that it does not fit inside the smallest zeolite pores, it could block moderately-sized pores preventing a full quantitative analysis, and that it displays substantial dynamics at ambient temperature. Through conventional, high-field, and low-temperature $^{19}F$ MAS NMR techniques various active sites have been identified, including previously hard-to-detect $Al^V$ Brønsted acid sites that are in low concentrations but apparently crucial for adsorption and thus catalytic activity. The local aluminium environments, which are generally deemed as the active sites or adjacent to active sites (BAS), are very similar for zeolites HY and HZSM-5 in terms of where 3-fluoropyridine is bound; their $^{27}Al$ NMR signatures after polarisation transfer from $^{19}F$ are almost identical. However, the $^{19}F$ NMR response from the fluoropyridine is very different. This method provides valuable insight into different activity for seemingly similar sites. This concept is well known for zeolites, but not so well understood. Such findings provide further evidence for the nuanced role of zeolite active site environments in determining molecular interactions, reinforcing the need for detailed

 

spectroscopic characterisation to fully understand structure–function relationships in zeolite catalysis.

## Experimental procedures

Details regarding the experimental procedures can be found in the ESI.†

## Data availability

Data for this article, including NMR and FT-IR data are available at Figshare at **https://doi.org/10.48420/28378607.v1**.

## Author contributions

D. L. conceptualized the original idea. J. H., Y. M., and R. Z. designed the adsorption conditions and performed the standard characterization of all samples. J. H. collected, interpreted, and finalized the solid-state NMR data with input and supervision from P. C. V. for the low temperature MAS NMR and from D. I. for the high-field MAS NMR. S. Y. and X. F. supervised the synthetic and adsorption work and D. L. supervised the solid-state NMR spectroscopy. J. H. wrote the first draft of the manuscript and the ESI.† S. Y., X. F., and D. L. revised the article for submission, with input from all coauthors.

## Conflicts of interest

The authors declare no competing interests.

## Acknowledgements

The UK High-Field Solid-State NMR Facility used in this research was funded by EPSRC and BBSRC (EP/T015063/1), as well as the University of Warwick including *via* part funding through Birmingham Science City Advanced Materials Projects 1 and 2 supported by Advantage West Midlands (AWM) and the European Regional Development Fund (ERDF). The low temperature (100 K) MAS NMR experiments were performed at the Nottingham DNP MAS NMR Facility which is funded by the University of Nottingham and EPSRC (EP/L022524/1 and EP/R042853/1). We also thank the EPSRC and The University of Manchester for funding the 16.4 T NMR spectrometer (EP/V007580/1) used in this work.

## References

1 K. Li, J. Valla and J. Garcia-Martinez, *ChemCatChem*, 2014, **6**, 46–66.
2 M. Niwa, K. Suzuki, N. Morishita, G. Sastre, K. Okumura and N. Katada, *Catal. Sci. Technol.*, 2013, **3**, 1919–1927.
3 N. Rahimi and R. Karimzadeh, *Appl. Catal., A*, 2011, **398**, 1–17.
4 A. Primo and H. Garcia, *Chem. Soc. Rev.*, 2014, **43**, 7548–7561.
5 M. Dusselier, M. A. Deimund, J. E. Schmidt and M. E. Davis, *ACS Catal.*, 2015, **5**, 6078–6085.
6 S. Wang, Z. Qin, M. Dong, J. Wang and W. Fan, *Chem Catal.*, 2022, **2**, 1657–1685.
7 J. Liang, G. Shan and Y. Sun, *Renewable Sustainable Energy Rev.*, 2021, **139**, 110707.
8 M. Hu, C. Wang, Y. Chu, Q. Wang, S. Li, J. Xu and F. Deng, *Angew. Chem., Int. Ed.*, 2022, **61**, e202207400.
9 Z. Qie, H. Xiang, H. Xiang, R. Zou, A. Alhelali, H. Alhassawi, S. Ding, Y. Jiao, S. M. Holmes, A. A. Garforth, X. Gao, J. Wang and X. Fan, *Fuel*, 2024, **368**, 131532.
10 Z. Dong, W. Chen, K. Xu, Y. Liu, J. Wu and F. Zhang, *ACS Catal.*, 2022, **12**, 14882–14901.
11 J. Sun, J. Dong, L. Gao, Y.-Q. Zhao, H. Moon and S. L. Scott, *Chem. Rev.*, 2024, **124**, 9457–9579.
12 A. Abraham, S.-H. Lee, C.-H. Shin, S. B. Hong, R. Prins and J. A. van Bokhoven, *Phys. Chem. Chem. Phys.*, 2004, **6**, 3031–3036.
13 J. Dědeček, Z. Sobalík and B. Wichterlová, *Catal. Rev.*, 2012, **54**, 135–223.
14 S. Ramdas, J. M. Thomas, J. Klinowski, C. A. Fyfe and J. S. Hartman, *Nature*, 1981, **292**, 228–230.
15 S. Wang, Y. He, W. Jiao, J. Wang and W. Fan, *Curr. Opin. Chem. Eng.*, 2019, **23**, 146–154.
16 P. G. Blakeman, E. M. Burkholder, H.-Y. Chen, J. E. Collier, J. M. Fedeyko, H. Jobson and R. R. Rajaram, *Catal. Today*, 2014, **231**, 56–63.
17 J. Jae, G. A. Tompsett, A. J. Foster, K. D. Hammond, S. M. Auerbach, R. F. Lobo and G. W. Huber, *J. Catal.*, 2011, **279**, 257–268.
18 C. D. Chudasama, J. Sebastian and R. V. Jasra, *Ind. Eng. Chem. Res.*, 2005, **44**, 1780–1786.
19 Y. Li, T.-S. Chung, C. Cao and S. Kulprathipanja, *J. Membr. Sci.*, 2005, **260**, 45–55.
20 U. Olsbye, S. Svelle, M. Bjørgen, P. Beato, T. V. W. Janssens, F. Joensen, S. Bordiga and K. P. Lillerud, *Angew. Chem., Int. Ed.*, 2012, **51**, 5810–5831.
21 B. Xu, C. Sievers, S. B. Hong, R. Prins and J. A. van Bokhoven, *J. Catal.*, 2006, **244**, 163–168.
22 A. Palčić and V. Valtchev, *Appl. Catal., A*, 2020, **606**, 117795.
23 J.-Z. Qiu, J. Hu, J. Lan, L.-F. Wang, G. Fu, R. Xiao, B. Ge and J. Jiang, *Chem. Mater.*, 2019, **31**, 9413–9421.
24 B. Wei, X. Liu, Q. Chang, S. Li, H. Luo, K. Hua, S. Zhang, J. Chen, Z. Shao, C. Huang, H. Wang and Y. Sun, *Chem Catal.*, 2022, **2**, 2066–2076.
25 T. Zhang, Z. Chen, A. G. Walsh, Y. Li and P. Zhang, *Adv. Mater.*, 2020, **32**, 2002910.
26 M. Rahimi, E.-P. Ng, K. Bakhtiari, M. Vinciguerra, H. A. Ahmad, H. Awala, S. Mintova, M. Daghighi, F. Bakhshandeh Rostami, M. de Vries, M. M. Motazacker, M. P. Peppelenbosch, M. Mahmoudi and F. Rezaee, *Sci. Rep.*, 2015, **5**, 17259.
27 M. A. Snyder and M. Tsapatsis, *Angew. Chem., Int. Ed.*, 2007, **46**, 7560–7573.
28 Z. Yu, S. Li, Q. Wang, A. Zheng, X. Jun, L. Chen and F. Deng, *J. Phys. Chem. C*, 2011, **115**, 22320–22327.
29 S. Li, O. Lafon, W. Wang, Q. Wang, X. Wang, Y. Li, J. Xu and F. Deng, *Adv. Mater.*, 2020, **32**, 2002879.

30 N. Thomas, J. Dhainaut, A. Moissette, O. Lafon and G. N. Manjunatha Reddy, *J. Phys. Chem. C*, 2024, **128**, 10428–10439.
31 D. Ma, F. Deng, R. Fu, X. Han and X. Bao, *J. Phys. Chem. B*, 2001, **105**, 1770–1779.
32 M. Zheng, Q. Wang, Y. Chu, X. Tan, W. Huang, Y. Xi, Y. Wang, G. Qi, J. Xu, S. B. Hong and F. Deng, *J. Am. Chem. Soc.*, 2024, **146**, 29417–29428.
33 C. A. Fyfe, G. C. Gobbi, G. J. Kennedy, J. D. Graham, R. S. Ozubko, W. J. Murphy, A. Bothner-By, J. Dadok and A. S. Chesnick, *Zeolites*, 1985, **5**, 179–183.
34 Y. Ji, K. Chen, A. Hao and G. Hou, *J. Magn. Reson. Open*, 2025, **22**, 100182.
35 L. Peng, Y. Liu, N. Kim, J. E. Readman and C. P. Grey, *Nat. Mater.*, 2005, **4**, 216–219.
36 R. Verma, C. Singhvi, A. Venkatesh and V. Polshettiwar, *Nat. Commun.*, 2024, **15**, 6899.
37 P. Xiao, L. Wang, H. Toyoda, Y. Wang, K. Nakamura, J. Huang, R. Osuga, M. Nishibori, H. Gies and T. Yokoi, *J. Am. Chem. Soc.*, 2024, **146**, 31969–31981.
38 S. Li, A. Zheng, Y. Su, H. Fang, W. Shen, Z. Yu, L. Chen and F. Deng, *Phys. Chem. Chem. Phys.*, 2010, **12**, 3895–3903.
39 H. Fang, P. Kamakoti, J. Zang, S. Cundy, C. Paur, P. I. Ravikovitch and D. S. Sholl, *J. Phys. Chem. C*, 2012, **116**, 10692–10701.
40 H. Soscún, O. Castellano, J. Hernandez, F. Arrieta, Y. Bermúdez, A. Hinchliffe, M. R. Brussin, M. Sanchez, A. Sierraalta and F. Ruette, *J. Mol. Catal. A: Chem.*, 2007, **278**, 165–172.
41 S. Wannakao, C. Warakulwit, K. Kongpatpanich, M. Probst and J. Limtrakul, *ACS Catal.*, 2012, **2**, 986–992.
42 D. L. Bhering, A. Ramírez-Solís and C. J. A. Mota, *J. Phys. Chem. B*, 2003, **107**, 4342–4347.
43 X. Rozanska, R. A. van Santen, T. Demuth, F. Hutschka and J. Hafner, *J. Phys. Chem. B*, 2003, **107**, 1309–1315.
44 C. Liu, G. Li, E. J. M. Hensen and E. A. Pidko, *J. Catal.*, 2016, **344**, 570–577.
45 A. Zheng, L. Chen, J. Yang, M. Zhang, Y. Su, Y. Yue, C. Ye and F. Deng, *J. Phys. Chem. B*, 2005, **109**, 24273–24279.
46 A. V. Yakimov, M. Ravi, R. Verel, V. L. Sushkevich, J. A. van Bokhoven and C. Copéret, *J. Am. Chem. Soc.*, 2022, **144**, 10377–10385.
47 Z. Yu, A. Zheng, Q. Wang, L. Chen, J. Xu, J. P. Amoureux and F. Deng, *Angew. Chem., Int. Ed.*, 2010, **49**, 8657–8661.
48 C. A. Fyfe, J. L. Bretherton and L. Y. Lam, *J. Am. Chem. Soc.*, 2001, **123**, 5285–5291.
49 J. Jiao, J. Kanellopoulos, W. Wang, S. S. Ray, H. Foerster, D. Freude and M. Hunger, *Phys. Chem. Chem. Phys.*, 2005, **7**, 3221–3226.
50 A. Zheng, S.-B. Liu and F. Deng, *Solid State Nucl. Magn. Reson.*, 2013, **55–56**, 12–27.
51 Q. Zhao, W.-H. Chen, S.-J. Huang, Y.-C. Wu, H.-K. Lee and S.-B. Liu, *J. Phys. Chem. B*, 2002, **106**, 4462–4469.
52 H.-M. Kao and C. P. Grey, *Chem. Phys. Lett.*, 1996, **259**, 459–464.
53 W. L. Earl, P. O. Fritz, A. A. V. Gibson and J. H. Lunsford, *J. Phys. Chem.*, 1987, **91**, 2091–2095.
54 G. I. Kapustin, T. R. Brueva, A. L. Klyachko, S. Beran and B. Wichterlova, *Appl. Catal.*, 1988, **42**, 239–246.
55 F. Benaliouche, Y. Boucheffa, P. Ayrault, S. Mignard and P. Magnoux, *Microporous Mesoporous Mater.*, 2008, **111**, 80–88.
56 F. Jin and Y. Li, *Catal. Today*, 2009, **145**, 101–107.
57 E. Selli and L. Forni, *Microporous Mesoporous Mater.*, 1999, **31**, 129–140.
58 W. R. Gunther, V. K. Michaelis, R. G. Griffin and Y. Roman-Leshkov, *J. Phys. Chem. C*, 2016, **120**, 28533–28544.
59 I. G. Shenderovich, G. Buntkowsky, A. Schreiber, E. Gedat, S. Sharif, J. Albrecht, N. S. Golubev, G. H. Findenegg and H.-H. Limbach, *J. Phys. Chem. B*, 2003, **107**, 11924–11939.
60 X. Yi, H. H. Ko, F. Deng, S. B. Liu and A. Zheng, *Nat. Protoc.*, 2020, **15**, 3527–3555.
61 H.-M. Kao and C. P. Grey, *J. Phys. Chem.*, 1996, **100**, 5105–5117.
62 G. Li, C. Foo, R. Fan, M. Zheng, Q. Wang, Y. Chu, J. Li, S. Day, P. Steadman, C. Tang, T. W. B. Lo, F. Deng and S. C. E. Tsang, *Science*, 2025, **387**, 388–393.
63 J. B. Nicholas, J. F. Haw, L. W. Beck, T. R. Krawietz and D. B. Ferguson, *J. Am. Chem. Soc.*, 1995, **117**, 12350–12351.
64 A. Simon, L. Delmotte, J.-M. Chezeau and L. Huve, *Chem. Commun.*, 1997, 263–264.
65 A. Simon, L. Delmotte, J.-M. Cheźeau, A. Janin and J.-C. Lavalley, *Phys. Chem. Chem. Phys.*, 1999, **1**, 1659–1664.
66 J.-H. Yang, L. A. Clark, G. J. Ray, Y. J. Kim, H. Du and R. Q. Snurr, *J. Phys. Chem. B*, 2001, **105**, 4698–4708.
67 H.-M. Kao and Y.-C. Chen, *J. Phys. Chem. B*, 2003, **107**, 3367–3375.
68 C. Lee, D. J. Parrillo, R. J. Gorte and W. E. Farneth, *J. Am. Chem. Soc.*, 1996, **118**, 3262–3268.
69 M. Arabiourrutia, M. Olazar, R. Aguado, G. López, A. Barona and J. Bilbao, *Ind. Eng. Chem. Res.*, 2008, **47**, 7600–7609.
70 J. Qi, Y. Guo, H. Jia, B. Fan, H. Gao, B. Qin, J. Ma, Y. Du and R. Li, *Fuel Process. Technol.*, 2023, **240**, 107586.
71 A. Boréave, A. Auroux and C. Guimon, *Microporous Mater.*, 1997, **11**, 275–291.
72 E. Taarning, C. M. Osmundsen, X. Yang, B. Voss, S. I. Andersen and C. H. Christensen, *Energy Environ. Sci.*, 2011, **4**, 793–804.
73 S. C. Cardona and A. Corma, *Appl. Catal., B*, 2000, **25**, 151–162.
74 W. Song, R. E. Justice, C. A. Jones, V. H. Grassian and S. C. Larsen, *Langmuir*, 2004, **20**, 8301–8306.
75 K. Hadjiivanov, in *Advances in Catalysis*, ed. F. C. Jentoft, Academic Press, 2014, vol. 57, pp. 99–318.
76 V. Zholobenko, C. Freitas, M. Jendrlin, P. Bazin, A. Travert and F. Thibault-Starzyk, *J. Catal.*, 2020, **385**, 52–60.
77 R. Zhang, S. Xu, D. Raja, N. B. Khusni, J. Liu, J. Zhang, S. Abdulridha, H. Xiang, S. Jiang, Y. Guan, Y. Jiao and X. Fan, *Microporous Mesoporous Mater.*, 2019, **278**, 297–306.
78 C. V. Hidalgo, H. Itoh, T. Hattori, M. Niwa and Y. Murakami, *J. Catal.*, 1984, **85**, 362–369.
79 J. Cattanach, E. L. Wu and P. B. Venuto, *J. Catal.*, 1968, **11**, 342–347.

 

80 K. Chen, S. Horstmeier, Vy. T. Nguyen, B. Wang, S. P. Crossley, T. Pham, Z. Gan, I. Hung and J. L. White, *J. Am. Chem. Soc.*, 2020, **142**, 7514–7523.
81 D. J. Parrillo and R. J. Gorte, *J. Phys. Chem.*, 1993, **97**, 8786–8792.
82 J. W. Harris, W.-C. Liao, J. R. Di Iorio, A. M. Henry, T.-C. Ong, A. Comas-Vives, C. Copéret and R. Gounder, *Chem. Mater.*, 2017, **29**, 8824–8837.
83 W.-C. Liao, B. Ghaffari, C. P. Gordon, J. Xu and C. Copéret, *Curr. Opin. Colloid Interface Sci.*, 2018, **33**, 63–71.
84 I. B. Moroz, K. Larmier, W.-C. Liao and C. Copéret, *J. Phys. Chem. C*, 2018, **122**, 10871–10882.
85 S. Chapman, M. Carravetta, I. Miletto, C. M. Doherty, H. Dixon, J. D. Taylor, E. Gianotti, J. Yu and R. Raja, *Angew. Chem., Int. Ed.*, 2020, **59**, 19561–19569.
86 X. Wang, Q. Wang, C. Wang, Y. Chu, M. Hu, F. Deng, J. Yu and J. Xu, *J. Am. Chem. Soc.*, 2025, **147**, 17829–17838.